Energy-conserving low-order models for three-dimensional Rayleigh-Bénard convection

Christopher Tong
Department of Physics, Purdue University, West Lafayette, Indiana 47907-1396

Alexander Gluhovsky*
Department of Earth and Atmospheric Sciences, Purdue University, West Lafayette, Indiana 47907-1397

(Received 27 April 2001; revised manuscript received 7 December 2001; published 4 April 2002)

Constructing hydrodynamic low-order models in the form of coupled gyrostats eliminates the possibility of certain unphysical behaviors, such as solutions diverging to infinity, that often appear in models resulting from *ad hoc* truncations of Galerkin approximations. In this paper, a simple low-order model in a gyrostatic form that conserves energy in the dissipationless limit (Model I) is constructed for three-dimensional (3D) Rayleigh-Bénard convection. It can be considered an energy-conserving extension of the model by Das *et al.* [Phys. Rev. E **62**, R3051 (2000)] (Model II) that does not conserve energy and possesses solutions diverging to infinity. Also studied here is a smaller but energy-conserving subsystem of Model I that has the form of two coupled gyrostats (Model III). This new system is the 3D analog of the celebrated Lorenz model [J. Atmos. Sci. **20**, 130 (1963)]. Stability diagrams and heat transport behavior are calculated and compared for the three models. Model I has improved qualitative agreement with experimental observations compared to that of Model II and Model III.

DOI: 10.1103/PhysRevE.65.046306 PACS number(s): 47.20.Ky, 05.45.−a, 47.20.Bp, 47.54.+r

I. INTRODUCTION

Low-order models (LOMs) are low-dimensional dynamical systems, composed of ordinary differential equations, that are used to qualitatively investigate an underlying system of partial differential equations [1,2]. In theoretical fluid dynamics, LOMs have repeatedly shown their merit, as they have been used (for example) to demonstrate the possibility of chaos [3] and the spontaneous development of shearing instabilities [4] in thermal convection. A more recent example is the use of LOMs to understand a self-sustaining process in wall-bounded shear flows [5]. LOMs known as shell models are used to investigate turbulent cascade processes [6].

LOMs are commonly obtained by implementing a spectral Galerkin approximation. The hydrodynamic fields are expanded in infinite series of time-independent, orthogonal eigenfunctions that satisfy the boundary conditions. The series are then truncated and the remaining finite set of time-dependent ''Fourier'' coefficients satisfy a set of coupled, nonlinear ordinary differential equations (the LOM). This methodology has been pioneered by, e.g., Saltzman [7], Lorenz [1,3,8], and Obukhov [9]. Although the use of LOMs has a number of limitations, when carefully employed they continue to be successful in providing insights for hydrodynamic problems.

One limitation is that the modes retained in the truncations are often chosen in an *ad hoc* way, resulting in the possibility of unphysical behavior [10]. General principles for physically motivated choices are required. One proposal is to choose truncations resulting in LOMs that are formally equivalent to equations for coupled three-mode systems known in mechanics as *Volterra gyrostats*, in a forced, dissipative regime [11]. The Volterra gyrostat (e.g., [12]),

$$\begin{aligned} \dot{v}_1 &= pv_2v_3 + bv_3 - cv_2, \\ \dot{v}_2 &= qv_3v_1 + cv_1 - av_3, \\ \dot{v}_3 &= rv_1v_2 + av_2 - bv_1, \end{aligned} \tag{1}$$

where a, b, c, p, q, and r are constants such that $p+q+r=0$, and v_1, v_2, and v_3 are state variables that describe the dynamics of the system, can be thought of as a rigid body containing a rotor revolving with a constant angular velocity about an axis fixed in the carrier. Damping and forcing terms may be added to the system. The gyrostats that appear in LOMs are usually not of the general form (1) but rather one of its special cases. For instance, the widely known Lorenz model [3] has the form of Eq. (1) but with $r=b=c=0$ and with additional friction and forcing terms, as can be seen after a linear change of variables [11]. This version of the gyrostat will be referred to as the *Lorenz gyrostat*. Another gyrostat commonly encountered in LOMs is the *Euler gyroscope*, where $a=b=c=0$ so that only the three nonlinear terms are present. For a thorough discussion of Eqs. (1), including the relationships between the fluid dynamical and rigid bodies interpretations of the gyrostat, see [13].

Coupled gyrostats possess a number of features, shared with the underlying Navier-Stokes equations [13] that Obukhov [9] and Lorenz [3,8] considered desirable for LOMs: (i) they are quadratically nonlinear; (ii) in the dissipationless limit, they have at least one quadratic integral of motion; they also conserve state space volume (since $\Sigma_i \partial \dot{v}_i / v_i = 0$, which implies a Liouville theorem); (iii) their solutions are bounded (even when there is linear viscous friction and constant forcing). In the rigid body interpretation of Eqs. (1), there are two quadratic invariants corresponding to kinetic energy and squared angular momentum. In coupled

*Electronic address: aglu@purdue.edu

gyrostatic LOMs for fluid dynamical problems, quadratic integrals of motion may be interpreted as some sort of energy in three-dimensional (3D) problems (Sec. II C) or as the energy and the enstrophy in 2D problems (e.g., [14]). Meanwhile, the Liouville equation is known to be a general property of dissipationless hydrodynamic systems [15].

Moreover, LOMs in the form of coupled gyrostats possess a modular structure, with gyrostats as elementary ''building blocks.'' In other words, adding more physical effects in the fluid model, e.g., rotation, topography, and magnetic field, results in adding linear gyrostatic terms to existing gyrostats [13,16], while increasing the order of approximation adds additional gyrostats. In the usual *ad hoc* approach, it is usually unclear how to increase the order of approximation while preserving the conservation and boundedness properties indicated above. However, these properties are always preserved if the LOM is extended by modifying and/or adding gyrostat ''building blocks'' to the system.

In this paper we develop LOMs in the form of coupled gyrostats for *three-dimensional* Rayleigh-Bénard convection. This classical problem considers the buoyancy-driven circulation in a shallow layer of fluid contained between two horizontal, isothermal surfaces (the lower one kept at higher temperature than the upper one) in the presence of a constant vertical gravitational field (e.g. [17,18]). One of the earliest LOMs for Rayleigh-Bénard convection was that of Saltzman [7], which directly led to the Lorenz model [3]. Similar to nearly all subsequent studies, both authors assumed *two-dimensional* flow. There have also been several LOM studies of 3D convection [19–22]. However, except for [20], these studies did not explicitly implement the principle that total energy should be conserved by a LOM in the dissipationless limit (in this paper, ''energy conservation'' will always mean ''energy conservation in the dissipationless limit''). This principle has been advocated by several investigators (e.g., [9–11,13,23,24]) and is usually implemented in shell models [6].

In Sec. II, a LOM in the form of coupled gyrostats for the problem of 3D Rayleigh-Bénard convection (Model I) is derived. It contains, as a subsystem, an interesting LOM (Model II) recently introduced by Das *et al.* [22] to study 3D convection. It is shown, however, that Model II does not have the coupled gyrostats structure and, consequently, does not, in general, conserve energy. Another subsystem of Model I is the *simplest* LOM for 3D convection (Model III), the 3D analog of the Lorenz model. It is composed of two coupled Lorenz models, each representing motion in each horizontal direction, and similar to the original Lorenz model, it conserves energy. We also refer to Model III as the ''3D Lorenz model.''

The dynamics of the models is analyzed in Sec. III. Lack of energy conservation in Model II results in unphysical solutions diverging to infinity. As systems of coupled gyrostats, Model I and Model III, in contrast, do not have such undesirable behavior. Model III has multiple, neutrally stable, steady-state solutions in the same parameter region. On the other hand, Model's I stability regime diagram is more consistent with experimental results than that for Model III. Beyond the threshold for stable steady-state solutions, Model I has periodic solutions involving ''asymmetric squares,'' analogous to those found in Model II [22], but the heat transport behavior for this solution in Model I is more consistent with experimental results than it is in Model II. Conclusions are presented in Sec. IV.

II. THE MODELS

A. Model I: Derivation

Consider a layer of fluid confined between two stress-free horizontal surfaces at altitudes $z=0,h$. (The unit vectors $\mathbf{x}$, $\mathbf{y}$, $\mathbf{z}$ are associated with the spatial coordinates x,y,z, respectively.) Horizontal periodic boundary conditions, with periodicity $2L$, are assumed; define the aspect ratio $a=h/L$. The temperature T is uniform on the $z=0$ surface with value T_0 and uniform on the $z=h$ surface with value $T_0-\delta T$, $\delta T>0$. The Oberbeck-Boussinesq equations [25] for the hydrodynamic fields $\mathbf{v}$ (velocity), p (pressure), and T are as follows:

$$\boldsymbol{\nabla}\cdot\mathbf{v}=0, \tag{2}$$

$$\frac{\partial\mathbf{v}}{\partial t}+(\mathbf{v}\cdot\boldsymbol{\nabla})\mathbf{v}=-\frac{\boldsymbol{\nabla}p}{\rho_0}-[1-\alpha(T-T_0)]g\hat{\mathbf{z}}+\nu\nabla^2\mathbf{v}, \tag{3}$$

$$\frac{\partial T}{\partial t}+(\mathbf{v}\cdot\boldsymbol{\nabla})T=\kappa\nabla^2 T, \tag{4}$$

where t is time and the following quantities are assumed constant: ν, the kinematic viscosity; κ, the thermal diffusivity; α, the thermal expansion coefficient; g, the gravitational field; and ρ_0, the mass density at $T=T_0$. These equations represent the balances of mass, momentum, and thermal energy, respectively. Let θ/π be the temperature deviation from the conductive steady-state profile. Also define the Rayleigh number as $R=\alpha g\delta T h^3/\kappa\nu$ and the Prandtl number as $\sigma=\nu/\kappa$. The Nusselt number, which characterizes the heat transport efficiency in a convecting fluid, is

$$\mathrm{Nu}=1-\frac{h}{\pi\delta T}\left\langle\left.\frac{\partial\theta}{\partial z}\right|_{z=0,h}\right\rangle, \tag{5}$$

where the angle brackets denote a horizontal area average. The evaluation of the partial derivative at $z=0$ and $z=h$ should give the same result, unless there is a heat source or sink within the layer, not just at the boundaries.

The equations in a dimensionless form are obtained by transformations [10]: x, y, and z are normalized by h/π, T is normalized by δT, and time is normalized by the fluid's Brunt-Väisälä period $\tau=\sqrt{h/(g\alpha\delta T)}$. Finally, pressure is normalized by $\rho_0 h^2/\pi^2\tau^2$ and the kinematic viscosity and thermal diffusivity are both normalized by $h^2/\pi^2\tau$. The resulting nondimensional equations (in vorticity form) are as follows:

$$\boldsymbol{\nabla}\cdot\mathbf{v}=0, \tag{6}$$

$$\boldsymbol{\nabla}\times\mathbf{v}=\boldsymbol{\zeta}, \tag{7}$$

$$\frac{\partial \boldsymbol{\zeta}}{\partial t}=(\boldsymbol{\zeta}\cdot\boldsymbol{\nabla})\mathbf{v}-(\mathbf{v}\cdot\boldsymbol{\nabla})\boldsymbol{\zeta}+\nu\nabla^2\boldsymbol{\zeta}+\left(\mathbf{x}\frac{\partial\theta}{\partial y}-\mathbf{y}\frac{\partial\theta}{\partial x}\right), \tag{8}$$

$$\frac{\partial\theta}{\partial t}=-\mathbf{v}\cdot\boldsymbol{\nabla}\theta+v_z+\kappa\nabla^2\theta, \tag{9}$$

with the Rayleigh and Prandtl numbers, respectively,

$$R=\frac{\pi^4}{\nu\kappa},\qquad \sigma=\frac{\nu}{\kappa}.$$

The stress-free boundary conditions at the top and bottom of the layer (now $z=0,\pi$) are as follows:

$$v_z|_{z=0,\pi}=\left.\frac{\partial v_x}{\partial z}\right|_{z=0,\pi}=\left.\frac{\partial v_y}{\partial z}\right|_{z=0,\pi}=\theta|_{z=0,\pi}=0.$$

Horizontal periodic boundary conditions, with period $2\pi/a$, are also assumed.

Consider the following expansions in (truncated) Fourier series:

$$v_x=x_1(t)\sin(ax)\cos(z)+w_1(t)\sin(ax)\cos(ay)\cos(2z), \tag{10a}$$

$$v_y=y_1(t)\sin(ay)\cos(z)+w_1(t)\cos(ax)\sin(ay)\cos(2z), \tag{10b}$$

$$v_z=-ax_1(t)\cos(ax)\sin(z)-ay_1(t)\cos(ay)\sin(z)-aw_1(t)\cos(ax)\cos(ay)\sin(2z), \tag{10c}$$

$$\theta=\theta_{101}(t)\cos(ax)\sin(z)+\theta_{011}(t)\cos(ay)\sin(z)+\theta_{002}(t)\sin(2z)+\theta_{112}(t)\cos(ax)\cos(ay)\sin(2z)+\theta_{004}(t)\sin(4z). \tag{10d}$$

This choice retains a set of Lorenz [3] modes for each horizontal direction, plus one interaction mode each for velocity w_1 and temperature θ_{112}, and an additional mode θ_{004} whose role will be explained shortly. These expansions result in a low-order model with the following equations:

$$\dot{x}_1=-\nu(1+a^2)x_1-\frac{a}{1+a^2}\theta_{101}-\frac{a}{4}w_1y_1, \tag{11a}$$

$$\dot{y}_1=-\nu(1+a^2)y_1-\frac{a}{1+a^2}\theta_{011}-\frac{a}{4}w_1x_1, \tag{11b}$$

$$\dot{w}_1=-2\nu(2+a^2)w_1-\frac{a}{2+a^2}\theta_{112}+a\frac{1+a^2}{2+a^2}x_1y_1, \tag{11c}$$

$$\dot{\theta}_{101}=-\kappa(1+a^2)\theta_{101}-ax_1-ax_1\theta_{002} \tag{11d}$$

$$-\frac{a}{4}\theta_{112}y_1, \tag{11e}$$

$$\dot{\theta}_{011}=-\kappa(1+a^2)\theta_{011}-ay_1-ay_1\theta_{002}-\frac{a}{4}\theta_{112}x_1, \tag{11f}$$

$$\dot{\theta}_{002}=-4\kappa\theta_{002}+\frac{a}{2}\theta_{101}x_1+\frac{a}{2}\theta_{011}y_1, \tag{11g}$$

$$\dot{\theta}_{112}=-2\kappa(2+a^2)\theta_{112}-aw_1+\frac{a}{2}\theta_{011}x_1+\frac{a}{2}\theta_{101}y_1-2a\theta_{004}w_1, \tag{11h}$$

$$\dot{\theta}_{004}=-16\kappa\theta_{004}+\frac{a}{2}\theta_{112}w_1. \tag{11i}$$

This model has three parameters: a, the aspect ratio; ν, the nondimensional kinematic viscosity; and κ, the nondimensional thermal diffusivity. The critical Rayleigh number at which the conduction (trivial) solution loses stability is

$$R_c=\frac{\pi^4(1+a^2)^3}{a^2}, \tag{12}$$

and the normalized Rayleigh number is defined as $\tilde{r}=R/R_c$. Finally, the Nusselt number for the model becomes

$$\mathrm{Nu}=1-\left\langle\left.\frac{\partial\theta}{\partial z}\right|_{z=0,\pi}\right\rangle=1-2\theta_{002}-4\theta_{004}. \tag{13}$$

B. Model I: Coupled gyrostats structure

Consider the linear transformation of Model I (11) based on the following change of variables:

$$X=\frac{a}{\sqrt{2}}x_1,\quad \theta_2=-\frac{a^2}{\sqrt{2}(1+a^2)}\theta_{101},$$

$$Y=\frac{a}{\sqrt{2}}y_1,\quad \theta_3=-\frac{a^2}{\sqrt{2}(1+a^2)}\theta_{011},$$

$$W=\frac{a}{2}\sqrt{\frac{2+a^2}{1+a^2}}w_1,\quad \theta_4=\frac{a^2}{1+a^2}\theta_{004}+\left(\frac{1+2a^2}{2(1+a^2)}\right), \tag{14}$$

$$\theta_1=\frac{a^2}{1+a^2}\theta_{002}+\left(\frac{1+2a^2}{1+a^2}\right),\quad \theta_5=-\frac{a^2}{2(1+a^2)}\theta_{112}.$$

In the new variables, model (11) exhibits the structure of six coupled gyrostats

$$
\begin{array}{l|l|l|l|l|l|l|l|}
\dot{\theta}_1 = f_1 - \alpha_1 \theta_1 & -\theta_2 X & & -\theta_3 Y, & & & & \\
\dot{\theta}_2 = -\alpha_2 \theta_2 & +\theta_1 X & -X & & & & -\frac{1}{2}\theta_5 Y, & \\
\dot{X} = -\alpha_x X & & +\theta_2 & & & & & -\frac{\beta}{2} YW, \\
\dot{\theta}_3 = -\alpha_3 \theta_3 & & & +\theta_1 Y & -Y & & & \\
\dot{Y} = -\alpha_y Y & & & & +\theta_3 & & & -\frac{\beta}{2} WX, \\
\dot{\theta}_4 = f_2 - \alpha_4 \theta_4 & & & & & -2\beta\theta_5 W, & & \\
\dot{\theta}_5 = -\alpha_5 \theta_5 & & & & & +2\beta\theta_4 W & -\beta W & +\frac{1}{2}\theta_3 X \quad +\frac{1}{2}\theta_2 Y, \\
\dot{W} = -\alpha_w W & & & & & & +\beta\theta_5 & +\beta XY, \\
 & \text{I} & & \text{II} & & \text{III} & \text{IV} & \text{V} \quad \text{VI}
\end{array}
\tag{15}
$$

where $\alpha_1 = 4\kappa$, $\alpha_2 = \alpha_3 = \kappa(1+a^2)$, $\alpha_4 = 16\kappa$, $\alpha_5 = 2\kappa(2+a^2)$, $\alpha_x = \alpha_y = \nu(1+a^2)$, $\alpha_w = 2\nu(2+a^2)$, $f_1 = 4\kappa(1+2a^2)/(1+a^2)$, $f_2 = 2f_1$, and $\beta = \sqrt{(1+a^2)/(2+a^2)}$. The vertical bars are used to organize the model into a superposition of gyrostat "building blocks." It is evident that the model can be decomposed into six gyrostats: I and II are Lorenz gyrostats involving X, θ_1, θ_2 and Y, θ_1, θ_3, respectively; III is another Lorenz gyrostat involving W, θ_4, θ_5; IV and V are degenerative Euler gyroscopes involving X, θ_3, θ_5 and Y, θ_2, θ_5, respectively; and VI is an Euler gyroscope involving only the three velocity modes X, Y, and W. The remaining terms on the immediate right of the equal signs represent friction (the α's) and external forcing (f_1 and f_2) in the gyrostat interpretation.

C. Model I: Conservation of energy

It can be easily seen that in any system of coupled gyrostats, the sum of squares Σx_i^2 of all variables is conserved in the absence of forcing and friction, which guarantees boundedness of solutions [13]. In Rayleigh-Bénard convection, this quantity is simply related to the kinetic energy, total potential energy, and the available potential energy, respectively, in nondimensional variables

$$K = \frac{1}{2}\int_V \mathbf{v}^2 dV,$$

$$U = -\int_V \theta z dV,$$

$$A = -\frac{1}{2}\int_V \theta^2 dV,$$

where the integration is over a volume V comprising one "cell" of the horizontally periodic fluid layer. The available potential energy A is the portion of U available for conversion into kinetic energy (see [13] for further discussion and references therein). In the limits $\nu \to 0$ and $\kappa \to 0$, the LOM should conserve both the total energy $K+U$ and the "unavailable energy" $U-A$ [13]. For Model I, these two quadratic integrals of motion are

$$K + U = (1+a^2)(x_1^2 + y_1^2) + \frac{1}{2}(2+a^2)w_1^2 + 4\theta_{002} + 2\theta_{004}, \tag{16a}$$

$$U - A = \theta_{101}^2 + \theta_{011}^2 + \frac{1}{2}\theta_{112}^2 + 2\theta_{002}^2 + 4\theta_{002} + 2\theta_{004}^2 + 2\theta_{004}, \tag{16b}$$

and are indeed both conserved in the dissipationless limit. (Here, some constant terms and common factors are ignored.) In the variables (14), the two quadratic energy invariants (in the dissipationless limit) take the form

$$K + U = X^2 + Y^2 + W^2 + 2\theta_1 + \theta_4,$$

$$U - A = \left(\frac{1+a^2}{a^2}\right)(\theta_1^2 + \theta_2^2 + \theta_3^2 + \theta_4^2 + \theta_5^2 - 2\theta_1 - \theta_4),$$

so that their linear combination,

$$(K+U) + \frac{a^2}{1+a^2}(U-A) = X^2 + Y^2 + W^2 + \theta_1^2 + \theta_2^2 + \theta_3^2 + \theta_4^2 + \theta_5^2, \tag{17}$$

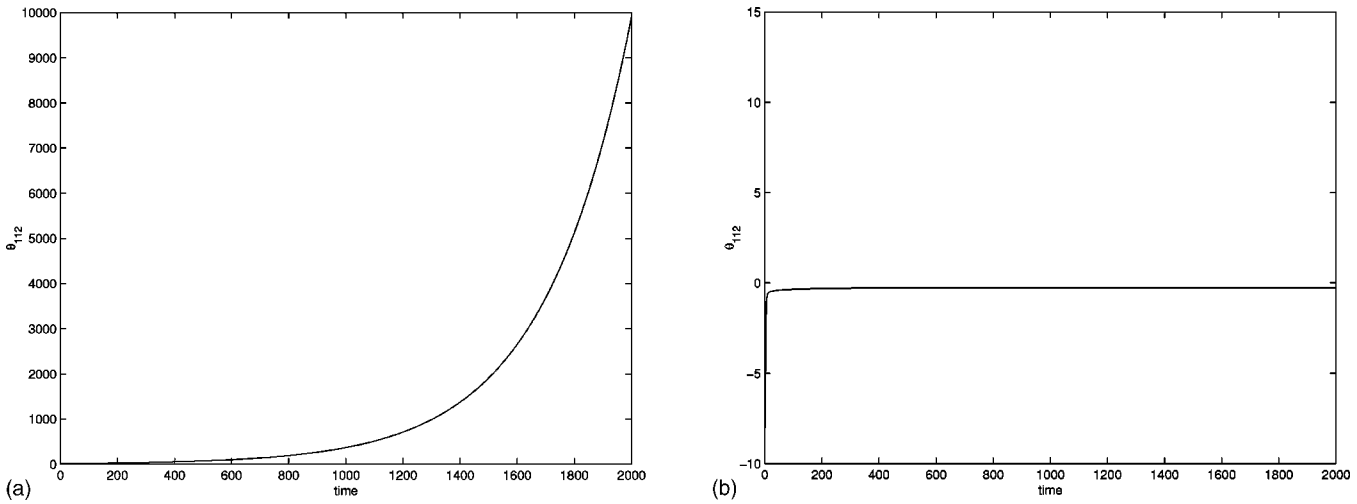

FIG. 1. Time series solution for θ_{112} in Model II (a) and Model I (b), with $a=1/\sqrt{2}$, $\sigma=10$, $\tilde{r}=19$, initial conditions $\theta_{112}(0)=10$, $w_1(0)=-10$, and all other variables zero. (All quantities are nondimensional.) The solution (a) illustrates the pathological divergence to infinity that is possible in Model II. In contrast, the solution for Model I (b) achieves an (unstable) steady state with $\theta_{112}\approx-0.2811$, $w_1\approx0.0570$, and $\theta_{004}\approx-0.0127$.

is also an integral of motion. This latter quantity is the aforementioned sum of squares of all the variables, which is always conserved in any system of coupled gyrostats.

Besides energy, there is another quadratic integral of motion for dissipationless 3D flow: the total helicity, $\mathbf{v}\cdot\boldsymbol{\zeta}/2$, integrated over V. However, in the truncations used for all models considered in this paper, the helicity is identically zero.

D. Model II

Excluding the θ_{004} term, representing the sin(4z) mode in the temperature expansion (10d), results in the seven-mode model recently introduced by Das *et al.* [22] (Model II). Note that Model II is actually a reduced version of the much larger model of Rucklidge and co-workers [21], which is also missing the important sin(4z) mode in the temperature expansion. The need for the sin(4z) mode is motivated by the fact that Model II has pathological solutions that exponentially diverge to infinity, such as the one illustrated in Fig. 1(a), while inclusion of the sin(4z) mode (that leads to Model I) removes the pathology, as illustrated in Fig. 1(b).

To gain insight into the reason behind this, note that Model II has an invariant manifold,

$$x_1=y_1=\theta_{101}=\theta_{011}=\theta_{002}=0, \tag{18}$$

on which the equations for the remaining variables, w_1 and θ_{112}, are linear and give unstable solutions for $R>R_{c2}=4\pi^4(2+a^2)^3/a^2$. Model I does not have this invariant manifold due to the presence of Eq. (11h) representing the sin(4z) mode.

To put it differently, lack of the sin(4z) mode in Model II makes it impossible to transform it into coupled gyrostats: nonlinear terms in gyrostat III are then absent while linear terms have the same (not opposite) sign, causing violation of the energy conservation. Indeed, with the sin(4z) mode missing in Model II, both the total energy $K+U$ and the "unavailable energy" $U-A$ are *not* conserved; in fact, in that model, the rate of change of energy in the dissipationless limit is

$$\frac{d}{dt}(K+U)=\frac{d}{dt}(U-A)=-a\,\theta_{112}(t)w_1(t),$$

which is not, in general, zero. In contrast, in Model I, the above rate of change is zero. Therefore, adding the sin(4z) mode to the temperature expansion (10d), restores conservation of energy and thus ensures that solutions are bounded.

These observations are similar to those for the Howard and Krishnamurti [4] model of 2D Rayleigh-Bénard convection with spontaneously generated vertical shear [24]. They clearly demonstrate that *one should never assume that a Galerkin approximation always conserves energy* in the dissipationless limit, although for 2D homogeneous incompressible flow, with *only mechanical* (not thermal) forcing, Galerkin approximations *do* conserve energy [8].

E. Model III (3D Lorenz model)

If the w_1, θ_{112}, and θ_{004} modes are removed from Eqs. (11), the resulting five-mode model constitutes the simplest model of three-dimensional Rayleigh-Bénard convection: the 3D analog of the Lorenz [3] model,

$$\dot{x}_1=-\nu(1+a^2)x_1-\frac{a}{1+a^2}\theta_{101}, \tag{19a}$$

$$\dot{y}_1=-\nu(1+a^2)y_1-\frac{a}{1+a^2}\theta_{011}, \tag{19b}$$

$$\dot{\theta}_{101}=-\kappa(1+a^2)\theta_{101}-ax_1-ax_1\theta_{002}, \tag{19c}$$

$$\dot{\theta}_{011}=-\kappa(1+a^2)\theta_{011}-ay_1-ay_1\theta_{002}, \tag{19d}$$

$$\dot{\theta}_{002} = -4\kappa\theta_{002} + \frac{a}{2}\theta_{101}x_1 + \frac{a}{2}\theta_{011}y_1, \tag{19e}$$

with Nusselt number $\mathrm{Nu} = 1 - 2\theta_{002}$. This five-mode system has the form of two coupled Lorenz models, one for each horizontal direction. This may be verified by restricting the flow to, say, the x-z plane ($y_1 \equiv \theta_{011} \equiv 0$). The resulting three-mode system is the original Lorenz model, as can be seen after a linear change of variables (e.g., [16]). Similarly, restricting the flow to the y-z plane ($x_1 \equiv \theta_{101} \equiv 0$) results in another three-mode Lorenz model. Therefore, including all five modes produces the *minimal* LOM for three-dimensional Rayleigh-Bénard convection. This five-mode model (19) will hereafter be referred to as the ''3D Lorenz model'' while the original three-mode Lorenz model [3] will be called the ''2D Lorenz model.'' We are not aware of any previous studies of the 3D Lorenz model, despite the fact that it is a simple and natural generalization of the 2D Lorenz model.

In variables (14), the 3D Lorenz model (19) becomes a system of two coupled Lorenz gyrostats I and II, where the first one describes motion in the x-z plane and the second one describes motion in the y-z plane. The associated friction and forcing terms are also present

$$\begin{array}{l|ll|ll}
\dot{\theta}_1 = f_1 - \alpha_1\theta_1 & -\theta_2 X & & -\theta_3 Y, & \\
\dot{\theta}_2 = -\alpha_2\theta_2 & +\theta_1 X & -X, & & \\
\dot{X} = -\alpha_x X & +\theta_2, & & & \\
\dot{\theta}_3 = -\alpha_3\theta_3 & & & +\theta_1 Y & -Y, \\
\dot{Y} = -\alpha_y Y & & & & +\theta_3, \\
 & \multicolumn{2}{c|}{\mathrm{I}} & \multicolumn{2}{c}{\mathrm{II}}
\end{array} \tag{20}$$

where f_1 and the α's are as before. The same linear combination (17), without the W, θ_4, θ_5 terms, is an integral of motion here and has the form of the sum of squares of all the variables.

The 3D Lorenz model (19) also conserves both total energy and ''unavailable energy'' in the limits $\nu \to 0$ and $\kappa \to 0$, since in this case, the quantities $K+U$ and $U-A$ are the evident modifications of those in Eqs. (16) (set $w_1 = 0$, $\theta_{112} = 0$, and $\theta_{004} = 0$). It is also known that the original 2D Lorenz model conserves the same two integrals of motion [13].

In the dissipationless limit ($\nu \to 0$ and $\kappa \to 0$), system (20) has a Hamiltonian structure with Hamiltonian,

$$H = \frac{1}{2}(X^2 + Y^2 + \theta_1^2 + \theta_2^2 + \theta_3^2),$$

the generalized Poisson bracket,

$$[f,g] = \frac{\partial f}{\partial x}\frac{\partial g}{\partial \theta_2} + \frac{\partial f}{\partial y}\frac{\partial g}{\partial \theta_3} - \frac{\partial f}{\partial \theta_1}\left(x\frac{\partial g}{\partial \theta_2} + y\frac{\partial g}{\partial \theta_3}\right) + \frac{\partial f}{\partial \theta_2}\left(x\frac{\partial g}{\partial \theta_1} - \frac{\partial g}{\partial x}\right) + \frac{\partial f}{\partial \theta_3}\left(y\frac{\partial g}{\partial \theta_1} - \frac{\partial g}{\partial y}\right),$$

for any two functions f and g, and the Casimir invariant,

$$C = X^2 + Y^2 + 2\theta_1,$$

which satisfies $[C,g] = 0$ for any g.

The Euler gyroscope, a three-dimensional rigid body, has an analog on the Lie algebra of group SO(n), which can be interpreted as an n-dimensional Euler gyroscope [26]. Similarly, the Volterra equations for a three-dimensional rigid body can be generalized to n dimensions [11]. System (20) was formulated in [11] as an example of the four-dimensional gyrostat.

III. DYNAMICS

A. Analysis of the 3D Lorenz model (Model III)

Similar to the 2D Lorenz model [3], the 3D Lorenz model has a conduction steady state (where all variables are zero) that loses stability at the critical Rayleigh number R_c given by Eq. (12), which has its minimum value, $27\pi^4/4$, at the critical aspect ratio $a_c = 1/\sqrt{2}$. This regime also results from the stability analysis of the original Oberbeck-Boussinesq equations [27].

Above the critical Rayleigh number, there are an infinite number of nontrivial steady-state solutions, all of which have the form

$$x_1^2 + y_1^2 = \frac{8}{\sigma(1+a^2)^2}\left(1 - \frac{R_c}{R}\right), \tag{21a}$$

$$\theta_{101} = -x_1\sqrt{\frac{R_c}{R}[\sigma(1+a^2)]}, \tag{21b}$$

$$\theta_{011} = -y_1\sqrt{\frac{R_c}{R}[\sigma(1+a^2)]}, \tag{21c}$$

$$\theta_{002} = -\left(1 - \frac{R_c}{R}\right), \tag{21d}$$

and the following relation between the Nusselt and Rayleigh numbers:

$$\mathrm{Nu} = 1 + 2\left(1 - \frac{R_c}{R}\right), \tag{22}$$

which again agrees with the corresponding result for the secondary (roll) solution of the 2D Lorenz model as well as the stability analysis of the Oberbeck-Boussinesq equations [28]. Finally, all steady states (21) are neutrally stable in the *same* parameter region, $1 < \tilde{r} < \tilde{r}_0$, where

$$\tilde{r}_0 = \frac{\sigma(\sigma + b + 3)}{\sigma - b - 1} \tag{23}$$

and $b = 4/(1+a^2)$. This is the same secondary critical Rayleigh number at which the roll solution loses stability in the 2D Lorenz model [3]. In Model III, roll solutions occur in either the x-z or y-z planes. In addition, solutions (21) in-

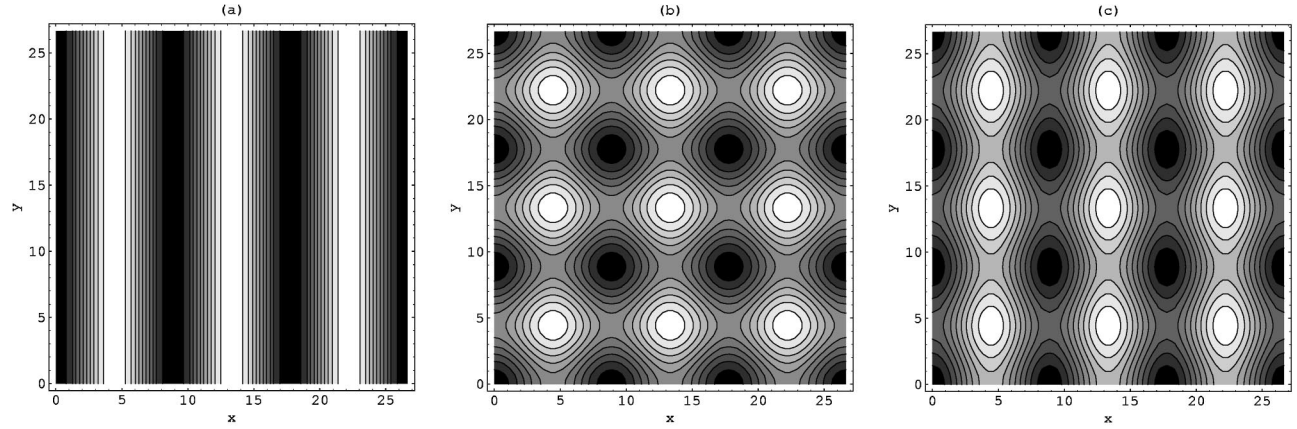

FIG. 2. Contour plots of vertical velocity at midplane ($z=\pi/2$) for neutrally stable steady-state solutions of the 3D Lorenz model (Model III): (a) roll planform, (b) symmetric square planform, and (c) ''asymmetric square'' planform. Axes scales are nondimensional.

clude 3D patterns: symmetric square convection cells, and intermediate planforms that could be characterized as asymmetric square cells, similar to those observed by Das *et al.* [22] in a time-varying regime of Model II. Both 2D and 3D solutions of Model III are shown in Fig. 2. It should be noted that weakly nonlinear convection only has the roll form at onset [17,18], in contrast to the situation in Model III.

Experimentally, the observation of both 2D and 3D convection patterns in the same parameter region has been observed [29], although in this case the 3D pattern is not a steady state, but a regime of spiral defect chaos. On the other hand, Eq. (23) has pathological features such as an asymptote at $\sigma=b+1$. For Prandtl numbers below this asymptote, steady-state solutions never lose stability [3]. In addition, for large Prandtl numbers, the expression in Eq. (23) increases linearly with Prandtl number, contradicting experimental results that suggest that $\tilde{r}_0$ approaches a plateau [30] with a theoretical upper bound at $\tilde{r}\approx 13$ [31]. Model I is free of these pathologies of the secondary critical Rayleigh number, as will be seen in the following section.

At Rayleigh numbers just beyond $\tilde{r}_0$, the 3D Lorenz model appears to have chaotic solutions similar to those in the 2D Lorenz model. Rather than probing the 3D Lorenz model in the supercritical regime, we turn next to the more adequate (for convection) Model I.

B. Analysis of Model I

As in the 2D and 3D Lorenz models, Model I has a conductive steady state that loses stability at the critical Rayleigh number, Eq. (12), whose minimal value, $27\pi^4/4$, is achieved at the critical aspect ratio $a_c=1/\sqrt{2}$. Above the critical Rayleigh number, there is a regime of stable 2D roll solutions. The analytical form of these solutions is identical to those in the 2D and 3D Lorenz models; for instance, rolls parallel to the y axis have the following form:

$$x_1^2=\frac{8}{\sigma(1+a^2)^2}\left(1-\frac{R_c}{R}\right),$$

$$\theta_{101}=-x_1\sqrt{\frac{R_c}{R}[\sigma(1+a^2)]},$$

$$\theta_{002}=-\left(1-\frac{R_c}{R}\right),$$

and $y_1=w_1=\theta_{011}=\theta_{112}=\theta_{004}=0$. There is an analogous expression for rolls parallel to the x axis. The heat transport relation, Eq. (22), is satisfied by these roll solutions. Square solutions, those with symmetric square planforms, exist but appear to be always unstable.

The secondary critical (normalized) Rayleigh number $\tilde{r}_0$, at which the roll solution loses stability, has been estimated numerically for $a=1/\sqrt{2}$ over a range of Prandtl numbers. Representative values are listed in Table I and plotted in Fig. 3. (The solid curve in Fig. 3 illustrates the stability curve for steady-state solutions in the 2D and 3D Lorenz models.) These results are consistent with those of Das *et al.* [22] in Model II, for the parameter region $4<\sigma<12$ that they displayed in their Fig. 1.

Model I is free of the aforementioned pathologies in the behavior of $\tilde{r}_0$ present in the 2D and 3D Lorenz models. At very low Prandtl numbers, $\tilde{r}_0$ approaches a finite value around 10.83, and there does not appear to be an asymptote in the curve. On the other hand, at high Prandtl numbers $\tilde{r}_0$ grows very slowly and approaches another finite value, around 18.50. The shape of this curve is qualitatively similar to the one observed experimentally [30], with growth at low Prandtl numbers and approach to a plateau value at high Prandtl numbers.

Beyond $\tilde{r}_0$, Model I possesses periodic solutions involving ''asymmetric squares,'' very much similar to those observed by Das *et al.* in Model II [22]. The sequence of patterns is illustrated in Fig. 4. The periodic solution coexists with chaotic solutions in the same parameter regime, and it has (at least a small) basin of attraction.

Experimentally, oscillatory ''asymmetric squares'' convection has not been observed. This may be due to a small basin of attraction for this solution, to the stress-free vertical

TABLE I. Secondary critical (normalized) Rayleigh number $\tilde{r}_0$ at which the roll solution loses stability in the modified DGK model. (The critical aspect ratio $a=1/\sqrt{2}$ is used.)

Prandtl number (σ)	$\tilde{r}_0$ (± 0.01)
0.01	10.83
0.1	10.83
0.2	10.84
0.3	10.84
0.5	10.87
1.0	10.97
2.0	11.32
5.0	12.63
10.0	14.31
17.5	15.70
25.0	16.45
37.5	17.09
50.0	17.44
62.5	17.65
75.0	17.80
87.5	17.90
100.0	17.98
10^3	18.46
10^4	18.50

boundary conditions and/or periodic horizontal boundary conditions, or to the severity of the Galerkin truncation. Oscillatory convection of qualitatively different forms (e.g., traveling waves propagating along the rolls), where the amplitude of oscillation increases smoothly with Rayleigh number [32], are usually observed experimentally. Nonetheless, it is still instructive to study the oscillatory ''asymmetric squares'' state in Model I, following the lead of Das *et al.* [22].

The Nusselt number for this periodic solution is also periodic in time, as was also seen in Model II [22]. The time-averaged values of Nusselt number calculated at various Rayleigh numbers for $\sigma=1$ and 25 are shown in Fig. 5, where the solid curve represents the exact Nusselt number, Eq. (22), for the steady-state solution in the parameter regime where it is stable. The black dots (and gray dots) are mean Nusselt numbers for the periodic solution where it was found to exist for Model I and Model II, respectively. In Model II, periodic solutions were found to exist in a narrower band of Rayleigh numbers than in Model I. It can be seen that Model II predicts that the Nusselt number actually starts decreasing as the Rayleigh number is increased past the transition from steady state to periodic motion. This is not consistent with experimental results that show a continual increase in the Nu vs R curve (e.g., [30]), as would be expected based on Le Chatelier's principle. Model I data does not have this feature at the transition from steady state to periodic motion. For $\sigma=1$, Model I data instead exhibits a discrete transition (abrupt change in slope) at that transition [Fig. 5(a)]. Furthermore, at a period doubling bifurcation (starting at $\tilde{r}\approx 29$) Model I data levels off and even dips a very slight amount as $\tilde{r}$ is increased further. For $\sigma=25$ there is a gradual change in slope of the heat transport curve for both models [Fig. 5(b)], although Model I data is increasing and Model II data is decreasing. The corresponding mean Nu for the chaotic solutions is generally higher for a given σ and R.

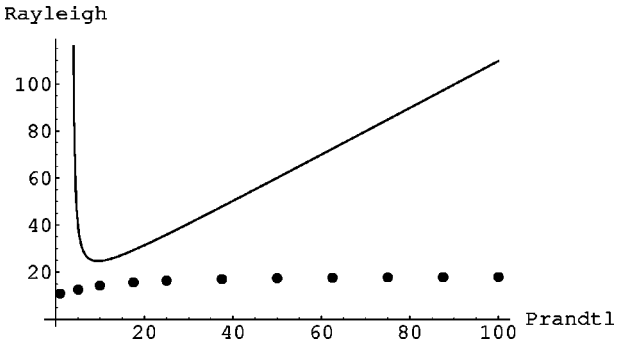

FIG. 3. Secondary critical (normalized) Rayleigh number $\tilde{r}_0$ as a function of Prandtl number σ for the 2D and 3D Lorenz models (solid curve) and Model I (points). (The critical aspect ratio $a=1/\sqrt{2}$ is used.) The stability boundary for Model I is better behaved than that for the Lorenz models at very low and very high Prandtl numbers, qualitatively consistent with experimental observations.

Experimentally, the idea of discrete transitions in the heat transport curve has been put forth by numerous authors (e.g., [30]), but Koschmieder [18] argues strongly that they do not really exist for shallow layer experiments (i.e., those performed in containers of very large aspect ratio). Particularly relevant to the model results discussed above are the low σ (helium) experiments of Ahlers and Behringer [33], which support Koschmieder's argument. (In fact, these studies [33] found a transition from steady-state to broadband time-dependent convection, not single-period convection, while monitoring the Nu signal.) Therefore, the discrete transition seen at $\sigma=1$ in Model I is probably an artifact of severe truncation.

Finally, it was observed that the amplitude of oscillation of the Nu signal generally increases with R in both Model I and Model II.

IV. CONCLUSION

In this paper, we have studied two simple low-order models for three-dimensional Rayleigh-Bénard convection: Model I and its subsystem, the 3D analog of the Lorenz model (Model III). These models have the form of coupled gyrostats, a structure that prevents certain unphysical behaviors that are manifested in LOMs constructed in a more *ad hoc* fashion, such as Model II.

The 3D Lorenz model (Model III) is the lowest-order nontrivial LOM for 3D thermal convection, and as such has intrinsic interest as a baseline for comparison with all higher-order models. Although the 3D Lorenz model leaves much to be desired, it is instructive to know exactly what can and cannot be accomplished with the simplest model of all.

The physical significance of our work on Model I is that we have found that the ''asymmetric squares'' oscillatory so-

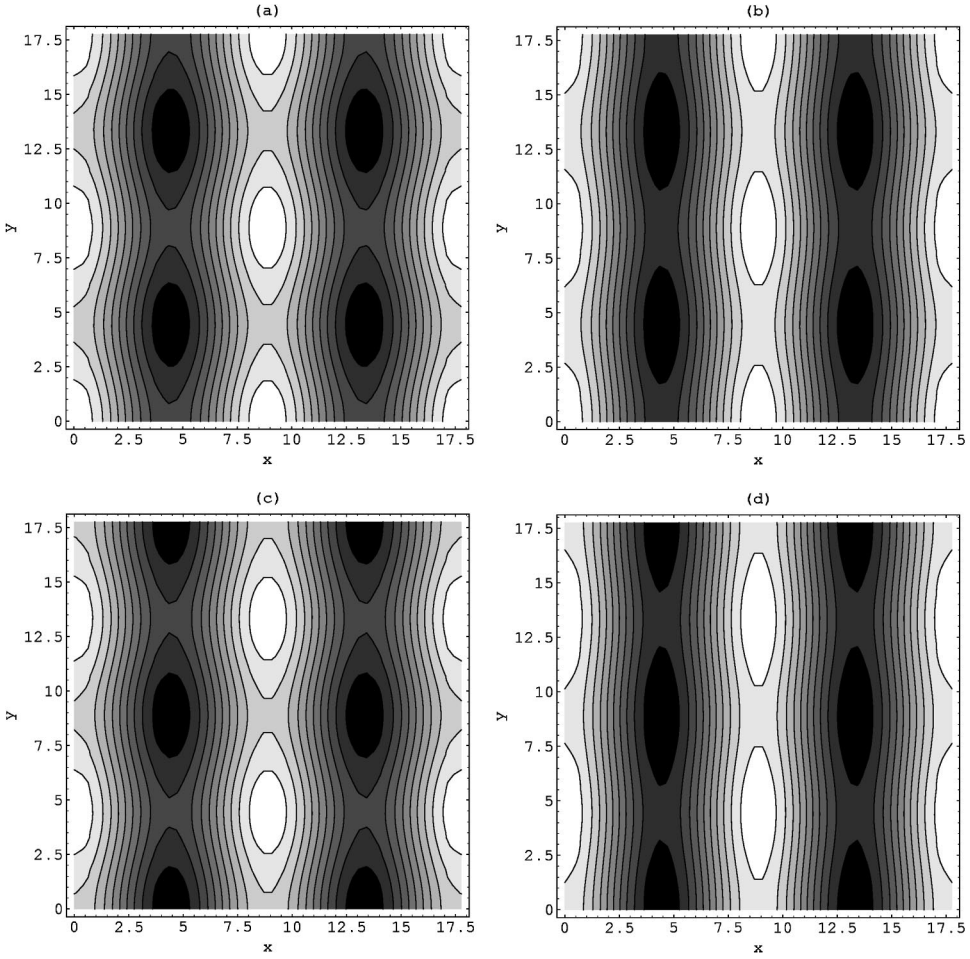

FIG. 4. Contour plots of vertical velocity at midplane ($z=\pi/2$) for a periodic solution of Model I at different times. The parameters are $\sigma=10$, $\tilde{r}=15$, and $a=1/\sqrt{2}$. The time sequence is (a) $\rightarrow$ (b) $\rightarrow$ (c) $\rightarrow$ (d). Axes scales are nondimensional.

lution discovered by Das *et al.* [22] is not merely the artifact of a problematic model. Our improved model eliminates unphysical behavior present in their model, and has heat transport behavior more consistent with experimental results and Le Chatelier's principle. Yet the ''asymmetric squares'' solution (not yet observed experimentally or in other theoretical/computational studies) persists in our improved model. This is evidence that further investigation of the ''asymmetric squares'' oscillation may hold promise.

The formal analogy between rigid body mechanics and fluid dynamics is well known (e.g., [26,34]). However, its manifestation in low-order models is usually in terms of coupled Euler gyroscopes, first suggested by Obukhov [9] to satisfy his requirements for *hydrodynamic type systems*: quadratic nonlinearity and conservation of energy and phase space volume in the absence of forcing and dissipation. Gyroscope ''triplets'' are also encountered in studies of nonlinear triadic interactions of helical waves [35]. However, the

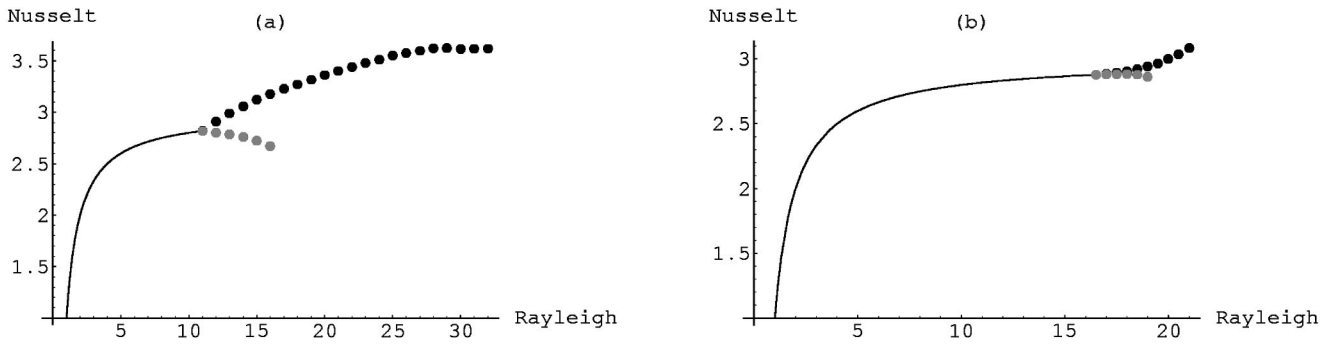

FIG. 5. Time-averaged Nusselt number (ratio of convective heat transfer to conductive heat transfer) for certain solutions of Models I and II, as a function of (normalized) Rayleigh number $\tilde{r}$ for Prandtl numbers $\sigma=1$ (a) and $\sigma=25$ (b), assuming $a=1/\sqrt{2}$. The solid curve represents the Nusselt number of the steady-state roll solutions in the regime where they are stable. The black dots are the numerically computed mean Nusselt numbers for periodic solutions of Model I when they are known to exist. The gray dots correspond to the corresponding data for Model II.

use of gyrostats allows a more general type of ''triplet,'' containing both nonlinear and linear terms, to be used as building blocks for LOMs. (The linear ''gyrostatic'' terms are needed to describe the effects of thermal forcing, as illustrated in any LOM of Rayleigh-Bénard convection, as well as effects such as rotation, topography, and magnetic field [13,16].) The use of coupled gyrostat LOMs may not be limited to the case of free-slip boundaries. Niederländer *et al.* [36] found that the Lorenz model (a single gyrostat [11]) is still usable in the rigid boundaries case.

The gyrostat analogy is not confined to low-order models, but occurs in a number of other areas in physics [37]. For instance, there are gyrostat analogies related to the dynamics of solid bodies with fluid-filled cavities [13,38], the static equilibrium of Euler elastica [39] and DNA molecules [40], the polarization dynamics of an optical pulse in a nonlinear medium [41], and quantum mechanics [42]. The Lorenz model, a special case of the gyrostat [11], itself has analogies in a number of diverse areas in physics [43]. Although much work in nonlinear dynamics is associated with coupled oscillators, it is suggested that coupled gyrostats should also receive attention as a fundamental nonlinear system.

ACKNOWLEDGMENTS

We are grateful to E. M. Agee and A. Tubis for their keen interest and helpful comments. We would also like to thank A. M. Rucklidge for valuable correspondence regarding [21] and M. Guenther for assistance with MATHEMATICA programming. This work was supported by National Science Foundation Grant No. ATM-9909009 and by the James S. McDonnell Foundation.

[1] E.N. Lorenz, J. Meteorol. Soc. Jpn. **60**, 255 (1982).
[2] *Nonlinear Hydrodynamic Modeling: A Mathematical Introduction*, edited by H. N. Shirer (Springer, Berlin, 1987); H. E. DeSwart, *Vacillation and Predictability Properties of Low-Order Atmospheric Spectral Models* (CWI, Amsterdam, 1989); P. Holmes, J. L. Lumley, and G. Berkooz, *Turbulence, Coherent Structures, Dynamical Systems and Symmetry* (Cambridge University Press, Cambridge, U. K., 1996).
[3] E.N. Lorenz, J. Atmos. Sci. **20**, 130 (1963).
[4] L.N. Howard and R. Krishnamurti, J. Fluid Mech. **170**, 385 (1986).
[5] F. Waleffe, Phys. Fluids **9**, 883 (1997); O. Dauchot and N. Vioujard, Eur. Phys. J.: Appl. Phys. **14**, 377 (2000).
[6] U. Frisch, *Turbulence: The Legacy of A. N. Kolmogorov* (Cambridge University Press, Cambridge, U. K., 1995); T. Bohr, M. H. Jensen, G. Paladin, and A. Vulpiani, *Dynamical Systems Approach to Turbulence* (Cambridge University Press, Cambridge, U. K., 1998).
[7] B. Saltzman, J. Atmos. Sci. **19**, 329 (1962).
[8] E.N. Lorenz, Tellus **12**, 243 (1960); J. Fluid Mech. **55**, 545 (1972).
[9] A.M. Obukhov, Dokl. Akad. Nauk. SSSR **14**, 32 (1969).
[10] Y.M. Treve and O.P. Manley, Physica D **4**, 319 (1982).
[11] A.B. Gluhovsky, Dokl. Akad. Nauk. SSSR **27**, 823 (1982).
[12] V. Volterra, Acta Math. **22**, 201 (1899).
[13] A. Gluhovsky and C. Tong, Phys. Fluids **11**, 334 (1999).
[14] A.B. Gluhovsky, Izv., Acad. Sci., USSR, Atmos. Oceanic Phys. **25**, 927 (1989).
[15] T.D. Lee, Q. Appl. Math. **10**, 69 (1952).
[16] A. Gluhovsky and E. Agee, J. Atmos. Sci. **54**, 768 (1997).
[17] A. V. Getling, *Rayleigh-Bénard Convection: Structures and Dynamics* (World Scientific, Singapore, 1998).
[18] E. L. Koschmieder, *Bénard Cells and Taylor Vortices* (Cambridge University Press, Cambridge U. K., 1993).
[19] J.B. McLaughlin and P.C. Martin, Phys. Rev. A **12**, 186 (1975); R.G. Kennett, Stud. Appl. Math. **55**, 65 (1976); J.H. Curry, J.R. Herring, J. Loncaric, and S.A. Orszag, J. Fluid Mech. **147**, 1 (1984); A.M. Rucklidge, Proc. R. Soc. London, Ser. A **453**, 107 (1997).
[20] H.N. Shirer, Beitr. Phys. Atmos. **59**, 126 (1986).
[21] P.C. Matthews, A.M. Rucklidge, N.O. Weiss, and M.R.E. Proctor, Phys. Fluids **8**, 1350 (1996); J.R. Gog, I. Oprea, M.R.E. Proctor, and A.M. Rucklidge, Proc. R. Soc. London, Ser. A **455**, 4205 (1999).
[22] A. Das, U. Ghosal, and K. Kumar, Phys. Rev. E **62**, R3051 (2000).
[23] J. A. Dutton, in *Nonlinear Hydrodynamic Modeling: A Mathematical Introduction*, edited by H. N. Shirer (Springer, Berlin, 1987); U. Achatz and G. Schmitz, J. Atmos. Sci. **54**, 2452 (1997); N. Gershenfeld, *The Nature of Mathematical Modeling* (Cambridge University Press, Cambridge, U. K., 1999).
[24] J.-L. Thiffeault and W. Horton, Phys. Fluids **8**, 1715 (1996).
[25] D. J. Tritton, *Physical Fluid Dynamics*, 2nd ed. (Clarendon, Oxford, 1988).
[26] V. I. Arnol'd, *Mathematical Methods of Classical Mechanics*, 2nd ed. (Springer, New York, 1989).
[27] J.W.S. Rayleigh, Philos. Mag. **32**, 529 (1916).
[28] W.V.R. Malkus and G. Veronis, J. Fluid Mech. **4**, 225 (1958).
[29] R.V. Cakmur, D.A. Egolf, B.B. Plapp, and E. Bodenschatz, Phys. Rev. Lett. **79**, 1853 (1997).
[30] R. Krishnamurti, J. Fluid Mech. **42**, 295 (1970); **42**, 309 (1970).
[31] F.H. Busse, J. Math Phys. **46**, 140 (1967).
[32] V. Croquette, Contemp. Phys. **30**, 113 (1989).
[33] G. Ahlers, Phys. Rev. Lett. **33**, 1185 (1974); R.P. Behringer and G. Ahlers, J. Fluid Mech. **125**, 219 (1982).
[34] J. E. Marsden and T. S. Ratiu, *Introduction to Mechanics and Symmetry*, 2nd ed. (Springer, New York, 1999).
[35] F. Waleffe, Phys. Fluids A **4**, 350 (1992); L. Turner, Phys. Rev. E **54**, 5822 (1996).
[36] J. Niederländer, M. Lücke, and M. Kamps, Z. Phys. B: Condens. Matter **82**, 135 (1991).
[37] W. Thomson, Nature (London) **15**, 297 (1877); A. Gray, *A Treatise on Gyrostatics and Rotational Motion* (Dover, New York, 1959); R.V.L. Hartley, Bell Syst. Tech. J. **29**, 350 (1950); **29**, 369 (1950).
[38] N. N. Moiseyev and V. V. Rumyantsev, *Dynamic Stability of Bodies Containing Fluid* (Springer, New York, 1968).

[39] J. Larmor, Proc. London Math. Soc. **15**, 170 (1884); A. Mielke and P. Holmes, Arch. Ration. Mech. Anal. **101**, 319 (1988).
[40] E.L. Starostin, Meccanica **31**, 235 (1996).
[41] J. Larmor, Proc. London Math. Soc. **21**, 423 (1890); **23**, 127 (1892); M.V. Tratnik and J.E. Sipe, Phys. Rev. A **35**, 2965 (1987); D. David, D.D. Holm, and M.V. Tratnik, Phys. Rep. **187**, 281 (1990).
[42] I.V. Komarov and V.V. Zalipaev, J. Phys. A **17**, 1479 (1984); M. Ge, Z.F. Wang, and K. Xue, Phys. Lett. A **235**, 41 (1997).
[43] H. Haken, Phys. Lett. **53A**, 77 (1975); E. Knobloch, *ibid.* **82A**, 439 (1981); M. Gorman, P.J. Widmann, and K.A. Robbins, Physica D **19**, 255 (1986); D. Poland, *ibid.* **65**, 86 (1993); K.M. Cuomo and A.V. Oppenheim, Phys. Rev. Lett. **71**, 65 (1993); N. Hemati, IEEE Trans. Circuits Syst., I: Fundam. Theory Appl. **41**, 40 (1994); Q. Li and H. Wang, Phys. Rev. E **58**, R1191 (1998).